Letters in Applied NanoBioScience
Open-Access Journal (ISSN: 2284-6808)

Article
Volume 13, Issue 2, 2024, 62
https://doi.org/10.33263/LIANBS132.062

Evaluation of *In-vitro* Antidiabetic Activity of Quercetin Loaded Eudrgit S100/GMO Nanoparticles

Poournima Sankpal [1,*], Ashok Hajare [2], Vishwajeet Patil [3], Sanket Rathod [1], Prafulla Choudhari [1], Rajesh Jagtap [4]

1 Department of Pharmaceutical Chemistry, Bharati Vidyapeeth College of Pharmacy, Palus (M.S.), India
2 Department of Pharmaceutics, Bharati Vidyapeeth College of Pharmacy, Palus (M.S.), India
3 Department of Pharmaceutical Chemistry, Ashokrao Mane College of Pharmacy, Peth Vadgaon (M.S.), India
4 Department of Pharmaceutics, Y.D. Mane College of Pharmacy, Kagal (M.S.), India
* Correspondence: poournima6@gmail.com;

Scopus Author ID 57220649018
Received: 7.03.2023; Accepted: 28.05.2023; Published: 30.06.2024

Abstract: In this study, we worked on developing, formulating, and investigating quercetin Eudragit S100/GMO nanoparticles for *in-vitro* antidiabetic activity by glucose uptake method. Quercetin is an active formulated into nanoformulation to improve its water solubility and improve *in-vitro* antidiabetic activity. Nanoparticles were made using a probe sonicator, Eudragit S100, Glyceryl Monooleate (GMO), and poloxamer 188. Particle size, Zeta potential, Differential Scanning Colorimetry (DSC), X-ray diffraction (XRD), Entrapment efficiency, loading content, and *in-vitro* release are all used to characterize nanoparticles. They show approximately 78.82% encapsulation with an average size of 161.3±0.66 nm and zeta potential +24.5Mv. The cumulative *in-vitro* drug release up to 12 hours was 90.12%, indicating that quercetin-loaded Eudragit S100 nanoparticles are effective for glucose absorption. The presence of active chemicals in the formulation of quercetin-loaded Eudragit S100 nanoparticles is responsible for greater antidiabetic efficacy by blocking carbohydrate-digesting enzymes with increased glucose absorption. As a result, it can potentially minimize postprandial hyperglycemia, and if the dosing regime is determined, it could be utilized to treat type 2 diabetes.

Keywords: diabetes; eudragit; quercetin; nanoparticles, *In-vitro.*

1. Introduction

Diabetes mellitus is a metabolic condition characterized by excessive blood sugar levels and improper carbohydrate, protein, and lipid metabolism [1]. Insulin deficiency or insensitivity causes glucose to build up in the circulation, resulting in various secondary macro- and micro-vascular problems. Diabetes mellitus is becoming more common as a result of sedentary lifestyles and a resulting increase in obesity. Diabetes mellitus affects an estimated 171 million persons globally [2]. Pharmacotherapy for diabetes mellitus control includes oral hypoglycemic medications, insulin, and a combination approach [3,4]. The disadvantages of current medicines include harmful side effects and continuous use, which leads to decreased effectiveness [5,6]. With the side effects and limitations of present treatments, continuing research is being undertaken on natural sources to develop new formulations for the effective management of diabetes and its consequences [7-11]. Plant bioactive chemicals have been found to inhibit digestive enzymes by their ability to bind to enzyme protein [12-14]. In diabetes mellitus, dietary fibers and their gelatinous polysaccharides also play a key role in

lowering postprandial plasma glucose levels. Several studies have demonstrated that proper glycemic control reduces the prevalence of retinopathy, nephropathy, and neuropathy, among other conditions [15-17].

Flavonoids are a polyphenolic structured type of secondary metabolite found in plants. Flavanols (quercetin, kaempferol), flavones, anthocyanins, and flavanones are the most common subgroups; they have different activities such as antioxidant, hepatoprotective, diarrhea, dysentery, astringent, nasal hemorrhage, anti-inflammatory, anticarcinogenic, antidiabetic, antiviral, and anticancer properties [18-20]. The polyphenolic flavonoid quercetin was swiftly bacterial activity or hydrolysis in the small intestine in the antidiabetic activity to produce quercetin aglycones, which were then converted back into the sulfated form of quercetin[21,22]. Quercetin has become a research hotspot for its antioxidant qualities, according to the bibliometric Analysis of the Web of Science database, as it has higher activity than biomolecules such as Trolox and rutinandascorbyl [23]. Quercetin is also used to treat osteoporosis, several forms of malignancies, and antiviral and cardiovascular diseases. At the same time, due to poor water solubility, bioavailability, and stability in the physiological media, quercetin's usage in pharmaceutical formulations is limited [24-26].

One strategy to solve these issues is to use new nanotechnology-based technologies to entrap quercetin in biodegradable polymeric nanoparticles, which have been developed to increase quercetin bioavailability [27,28]. Delivery of bioactive chemicals has received more attention in recent decades, emphasizing the development of nanoparticles, which can be used to solubilize, target specific organs, protect, control release, and augment the action of a natural biomolecule[29-32]. The quercetin molecule has been successfully encapsulated in nanoformulation to treat many diseases[33]. Biodegradable polymers as drug carriers have unique properties like the ease of surface modification due to low toxicity, higher biocompatibility, and the ability to protect and increase the stability of the encapsulated medication. Eudragit S100 is a methacrylic acid and methyl methacrylate anionic copolymer. Glyceryl Monooleate (GMO)/Eudragit S100 is a surface-modified nanoparticulate system that includes GMO as a lipid component, Eudragit S100 as a polymer, and poloxamer 188 as a stabilizer [34,35,36].

The goal of this study was to design and evaluate selected Qu-loaded nanoparticles using quercetin as a model hydrophobic phytoconstituent into pharmaceutically suitable nanoformulation using a holistic approach against type 2 diabetes, taking into account the above-mentioned phytoconstituents mechanism of action. The potential antidiabetic effect of our planned nanoformulation was investigated using *In vitro* methods. The quality by design (QbD) approach can be utilized to get a better understanding of the process and formulation variables, resulting in product quality that is higher and more resilient while preserving the desired quality profile.

2. Materials and Methods

2.1. Chemicals.

Poloxamer 188 was purchased from BASF (Mumbai) Kolliphor®, MONEGYL®-0100 (GMO) from Mohini Organics Pvt. Ltd. (Mumbai). Quercetin was purchased from Loba Chemie., Eudragit S100, and the rest of the solvents and chemicals were obtained from Himedia Laboratories' Research Lab in Mumbai.

2.2. Formulation of nanoparticles.

2.2.1. Preparation of nanoparticles using central composite design.

The central composite design allows for the examination of a large number of independent variables in a small number of tests. A factorial design was used to explore the effect of changing the concentration of Eudragit S100 and poloxamer 188 on particle size and zeta potential. Batch number one was used for nanoparticle formulation according to the factorial design[37]. In molten 1.75 ml GMO, 100 mg of quercetin was dissolved. A total of 12.5 ml of 0.1 % poloxamer 188 was added dropwise and sonicated for 3 minutes at 18 W. A 2.4 % Eudragit S100 solution was added to the initial emulsion to produce the final nanoemulsion. The product was freeze-dried for 48 hours using percent mannitol as the cryoprotectant to generate a fine powder of nanoparticles. The whitish lyophilized product was then collected and stored at 4°C until needed[38,39].

2.3. Characterization of nanoparticles

2.3.1. Particle size and charge Measurements.

The mean polydispersity index and particle diameter of the nanoparticles were calculated using dynamic light scattering (Nanosizer N4 Plus, Beckman Coulter Inc., CA, USA). The electrical charge on the nanoparticles was measured using special electrophoresis (Zetasizer Zen Systems 3600, Malvern Instruments Ltd UK). The results were calculated in triplicate and shown as mean standard error.[40]

2.3.2. FTIR spectroscopy.

For the identification of functional groups contained in plant compounds, FTIR has shown to be a useful tool. By attaching an ATR accessory to an FTIR spectrometer, attenuated total reflection/Fourier transform infrared spectroscopy (ATR/FTIR) spectra were acquired at ambient temperature (Perkin Elmer, Spectrum 100)

2.3.3. Differential scanning calorimetry.

DSC was used to determine the phase behavior of quercetin, poloxamer 188, Eudragit S100, physical mixes, and Qu-loaded nanoparticles (2.0 mg 0.2). The thermal stability of CS nanoparticles was investigated using differential scanning calorimetry (DSC). (Hita., DSC-7020) In an aluminum pan, 3–5 mg of the sample was crimped at 10°C min-1 at a heating rate of 30 to 300°C[41].

2.3.4. X-ray diffraction analysis.

Quercetin, Poloxamer 188, Eudragit S100, and Qu-loaded were studied for XRD patterns. On a Rigaku Miniflex 600 with Cu K radiation at 40 kV and 45 mA backdrop, fewer sample holders were used to analyze nanoparticles. Diffractograms were acquired from 5° 80°utilizing a step size of 0.02°, a count time of 2s, and a scanning speed of 2°/min[42].

2.3.5. Determination of % entrapment efficiency and % drug loading.

Because insufficient trapping contributes to the drug's initial burst release, which could be attributable to the hydrophilicity of the Eudragit S100 polymer, entrapment efficiency has

been regarded as a significant metric. 20 mg of Qu-loaded nanoparticles were totally dissolved in 10 ml of DMSO. Before filtration, the resultant suspension was evaporated to remove any remaining solvent. The residue was then rinsed and diluted for 24 hours by gently shaking it at 37°C. The solution was then centrifuged at 16,000 g for 10 minutes, and the supernatant was collected. An aliquot (1 mL) of supernatant was diluted to 10 mL with DMSO, and absorbance was measured at 259 nm using a UV spectrophotometer. The percentages of quercetin encapsulated in nanoparticles (% EE) and (% LC) were computed as follows:

$$EE\ (\%) = \frac{Weight\ of\ quercetin\ in\ nanoparticles}{Initial\ weight\ of\ quercetin} \times 100$$

$$DL\ (\%) = \frac{Weight\ of\ quercetin\ in\ nanoparticles}{Weight\ of\ nanoparticles} \times 100$$

2.3.6 *In vitro* release studies.

An *in-vitro* study of Qu-loaded nanoparticles was used to measure the release of quercetin at a certain pH, and experiments were carried out in several simulated fluids at varied pH levels. The process involves immersing four milligrams of Qu-loaded in phosphate-buffered saline (PBS). For 12 hours, nanoparticles were suspended in PBS at various pH levels (2.0, 4.5, 6.8, and 7.4) in a dialysis membrane sac (MW cut-off 12 kDa; Sigma Aldrich). The encapsulated dialysis sac was submerged in 50 mL of PBS solution in a beaker. PBS; pH = 2.0 for the first four hours, pH = 4.5 for the following five to nine hours, pH = 6.8 for the next 10 hours, and lastly, pH = 7.4 for twelve hours. The 5 mL supernatant was collected in increments and examined on a 259 nm UV Spectrophotometer for quercetin estimation.[43,44]

2.4. Study of In-vitro antidiabetic activity (by glucose uptake yeast cell method)

The yeast suspension was made by washing it in distilled water many times until the supernatant fluids were clear (by centrifugation 3,000g× 5min). The supernatant fluid was used to make a 10% (v/v) suspension. 1 ml of 25 mM glucose solution was added to various quantities of extract (1000 g/ml) and incubated at 37°C for 10 minutes. The reaction was begun using 100 µl of yeast suspension, incubated, and vortexed for 60 minutes at 37°C. The reaction mixture was centrifuged (2,500g, 5 min) after 60 minutes, and glucose was measured spectrophotometrically at 565nm using the DNS method.[45] The following formula was used to compute the percentage increase in glucose absorption by yeast cells:

$$\%\ \text{increase of G uptake} = \frac{\text{Absorbance Control} - \text{Absorbance Sample}}{\text{AbsorbanceControl}} \text{x100}$$

The absorbance of the control reaction contains all reagents except test samples. The test sample's absorbance is the abs sample. Commercial baker's yeast (Easy Grow Baker's) was rinsed in distilled water several times before being centrifuged (3,000 g, 5 min) to achieve a clear supernatant. In addition, a 10% (v/v) suspension was made with the same. In 1 mL of glucose solution (5–25 mM), different amounts of both samples were added, and the mixture was incubated for 10 minutes at 37°C. The process was started by vortexing 100 liters of yeast suspension and incubating it at 37°C. Tubes were centrifuged (2500 g, 5 min) after 60 minutes,

and glucose was measured in the supernatant. Using the formula, the percentage increase in glucose absorption by yeast cells was computed [46,47].

3. Results and Discussion

3.1. Formulation of nanoparticles using a central composite design.

The goal of the study's optimization was to lower particle size with stable zeta potential. The optimum condition/central points (optimum) of the optimal combination regions were related to the following processing factors: Eudragit S 100 (gm) = 2.4 and Poloxamer 188 (gm) = 0.1. The overlay plot obtained by the experiment work was statistically examined using Design-Expert 11 software (Stat-Ease Inc., USA). ANOVA was used to determine the statistical accuracy of the polynomials.

Table 1. Summary of experimental design.

Std., Run	Factor 1	Factor 2	Response 1	Response 2
	A: Eudragit S 100 (gm)	B: Poloxamer 188 (gm)	Particle Size (nm)	Zeta potential (mV)
1	1.2	0.05	145	18.2
2	1.2	0.10	147	22.3
3	1.2	0.15	151	24.2
4	2.4	0.05	151	24.5
5	**2.4**	**0.10**	**172**	**24.9**
6	2.4	0.15	182	28.1
7	3.6	0.05	199	28.6
8	3.6	0.10	207	30.6
9	3.6	0.15	211	31.0

To examine the interaction of independent and dependent factors, counterplots, 3D response normal probability, surface graphs, and perturbation plots were developed. The in-range maximum, target, minimum, and none are used to optimize the formulation goal. The optimization techniques employed are both numerical and graphical.

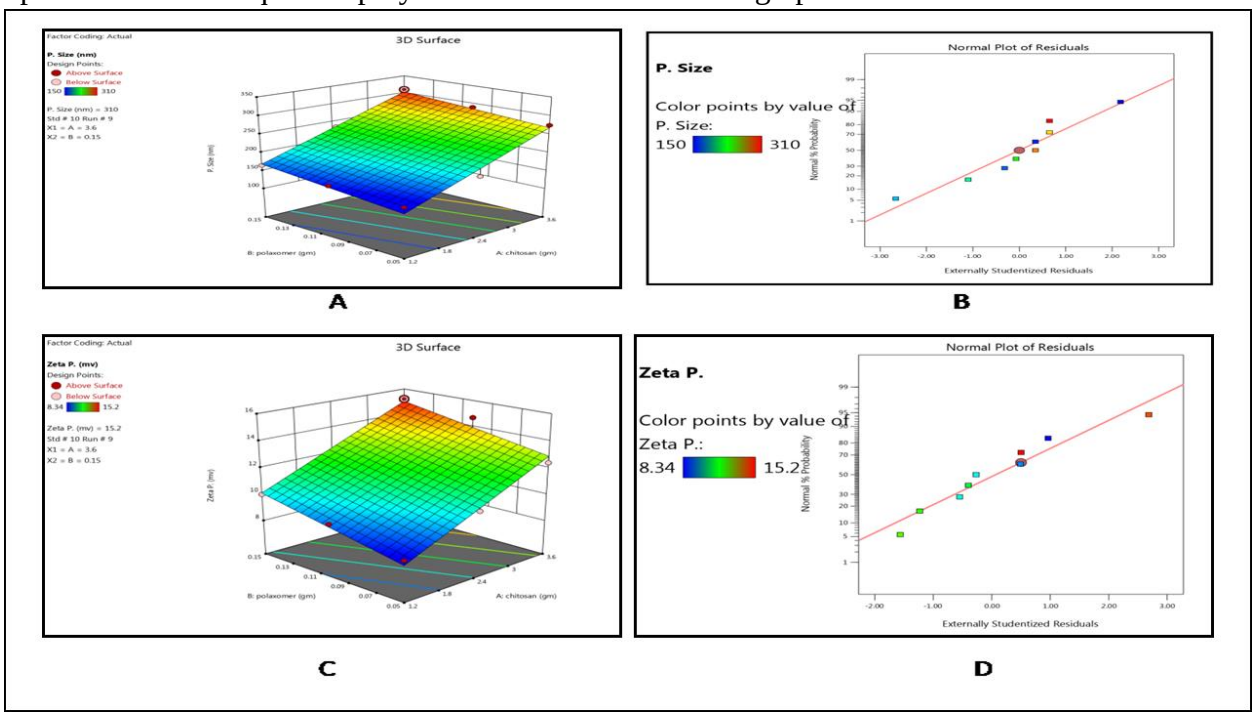

Figure 1. Central composite models of **(A)** 3-D plot of particle size **(B)** Normal residual plots **(C)** 3-D plot of zeta potential **(D)** Normal residual plots.

The following table 1 shows the criteria for nanoparticle optimization. Because the values of the center point provided by the overlay plot matched batch F5, it was chosen as the best batch.

Figure 1 shows two regions: a yellow region indicating a design space area with possible response values and a grey region describing an area where the answer did not satisfy the quality product standards. The ideal condition/central points of the best combination areas (optimum) for the processing factors Eudragit (mg) =2.4 %and poloxamer 188 (mg) = 0.1 %. These conditions were used to estimate the formulation of nanoparticles with (nm) = 218 and Zeta potential (mV) = 11.50.

3.2. Characterization of Qu-loaded nanoparticles

3.2.1. Analysis of particle size and zeta potential.

With PDI 0.148, the mean diameter of Qu-loaded nanoparticles was 161.30 nm. The surface charge of the particles has a zeta potential of +24.5 mV.

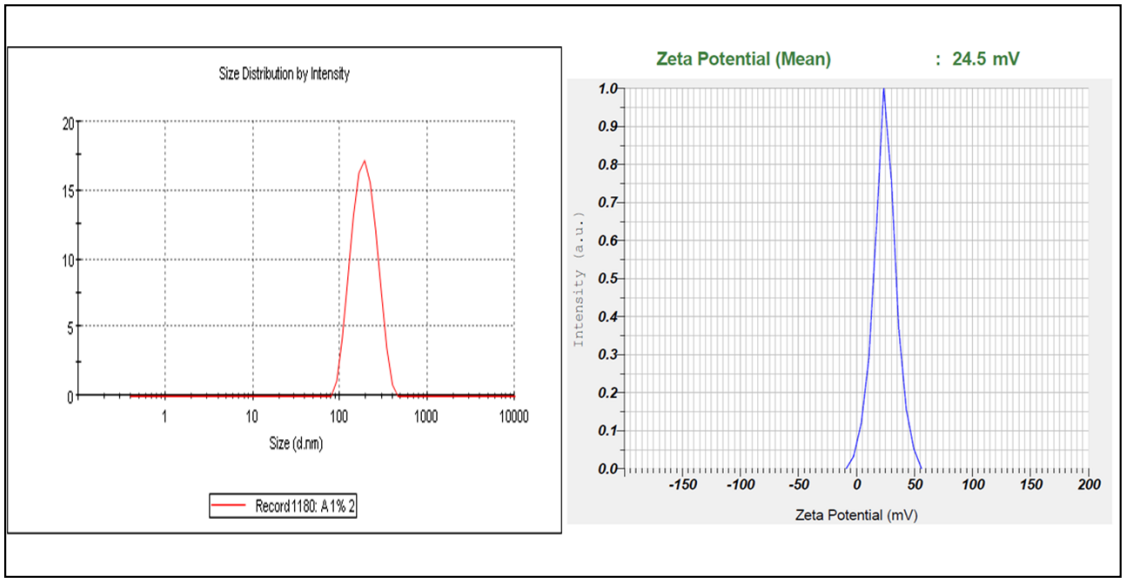

Figure 2. Particle size and zeta potential of quercetin nanoformulation.

3.2.2. FTIR of nanoparticles.

A spectrum of the characteristic peak formed by FTIR for the Eudragit S100 (Figure 3A) shows a stretch of carbonyl (ester) groups present in the Eudragit S100, and prominent bands may be seen in the spectra between 1150-1190 cm^{-1} and 1240-1270 cm^{-1}. At 1734.01 cm^{-1}, There are also C (=O) ester vibration stretching bands. The FTIR spectra bands 1388.22, 1449.97, 2953, and 2992.11cm^{-1} correspond to CHx vibration. OH stretch IR absorption frequency at 3437.91 cm^{-1} Poloxamer 188's carbon chain (Figure 3B) has an aliphatic C-H stretch of 2881.11 cm^{-1}, a plane O-H bend of 1365.12 cm^{-1} and 1242.02 cm^{-1}, a C-O stretch of 1096.99 cm^{-1}, and a CH=CR2 stretch of 840.46 cm^{-1}. GMO's C=O functionality was seen with a high peak at 1738 cm^{-1} (Figure 3C). Broadband at 3194.61 cm^{-1} is associated with OH stretching and hydrogen bonding between phenolic hydroxyl groups in quercetin (Figure 3D). 3190.38 cm–1 for O-H stretch, 2935.23 cm^{-1} for =C-H stretch, 1454.09 cm^{-1} for aromatic C=C stretch, and 1145.06 cm^{-1} for aromatic C-O stretch. At 1255.93 cm^{-1}, the COOH stretch/bend is seen. At 1454.44 cm–1, aromatic ring stretching is found; the C-O stretch is 1021.45 cm^{-1}.

The O-H stretch of quercetin was no longer visible in the spectra of Qu-loaded nanoparticles (Figure 3E). These findings revealed that intermolecular hydrogen bonding occurred in the nanoformulation, associated with less crystalline than quercetin. Several investigations have shown that hydrogen bonding can influence drug crystal transition to an amorphous state.

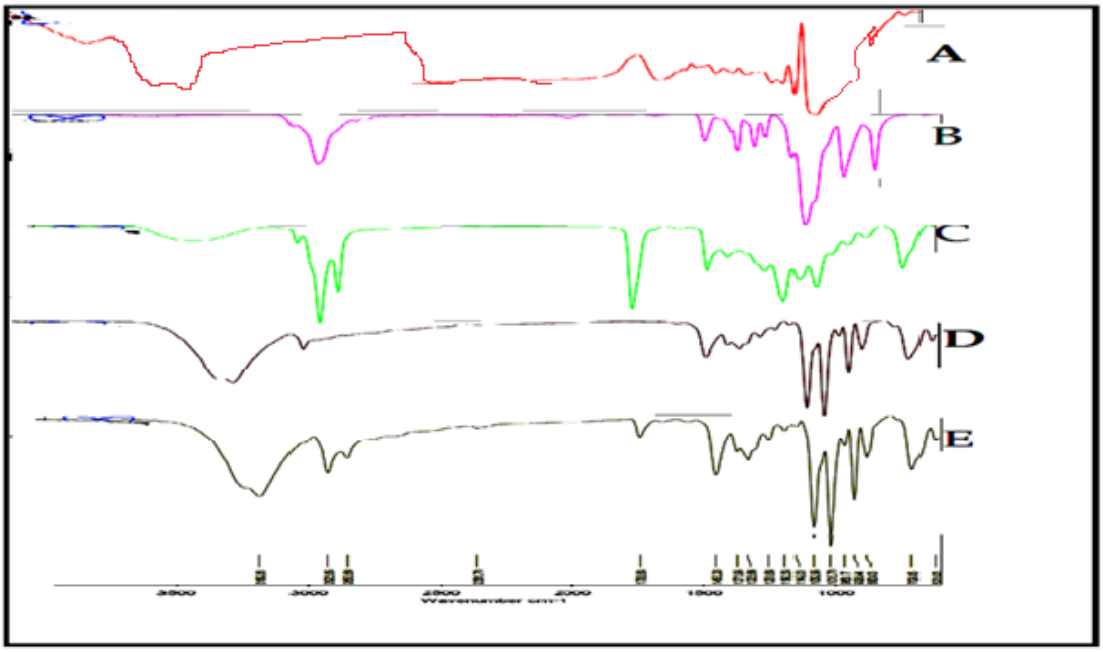

Figure 3. FTIR Spectra of Qu-loaded nanoparticles **(A)** Eudragit S100, **(B)** Poloxamer 188, **(C)** GMO, **(D)** Quercetin, **(E)** Quercetin nanoformulation

3.2.3. Differential scanning colorimetry.

Differential scanning calorimetry can provide information about the stability and physical and chemical properties of biomolecules placed into nanoparticles because it measures the temperature and energy variation in the phase transition of the material. As a result, the interaction between excipients and biomolecules can be determined by the disappearance of peaks at the same time as the development of new peaks that differ from the previous peaks in onset and shape. The emergence of a strong endothermic peak at 129.94°C was seen for quercetin (Figure 4A); the essential endothermic peak of poloxamer 188 (Figure 4B) was found to be at 58.92°C, which corresponded to its melting temperatures. While the Eudragit S100 thermogram showed a large endothermic peak between 87.13°C and 226°C (Figure 4C), the thermogram of a physical mixture of quercetin, poloxamer-188, and Eudragit S100 revealed no changes in the peaks of the mixture components, showing that there is no interaction between them (Figure 4D). The absence of the quercetin's characteristic peak in the thermogram of Qu-loaded nanoparticles (Figure 4E) indicates complete encapsulation in amorphous or molecular dispersion within the nanoparticles. Thus, DSC tests show the compatibility of a biomolecule with the remaining components in the suggested nanoformulation, and they agree well with FT-IR and PXRD results.(48.49)

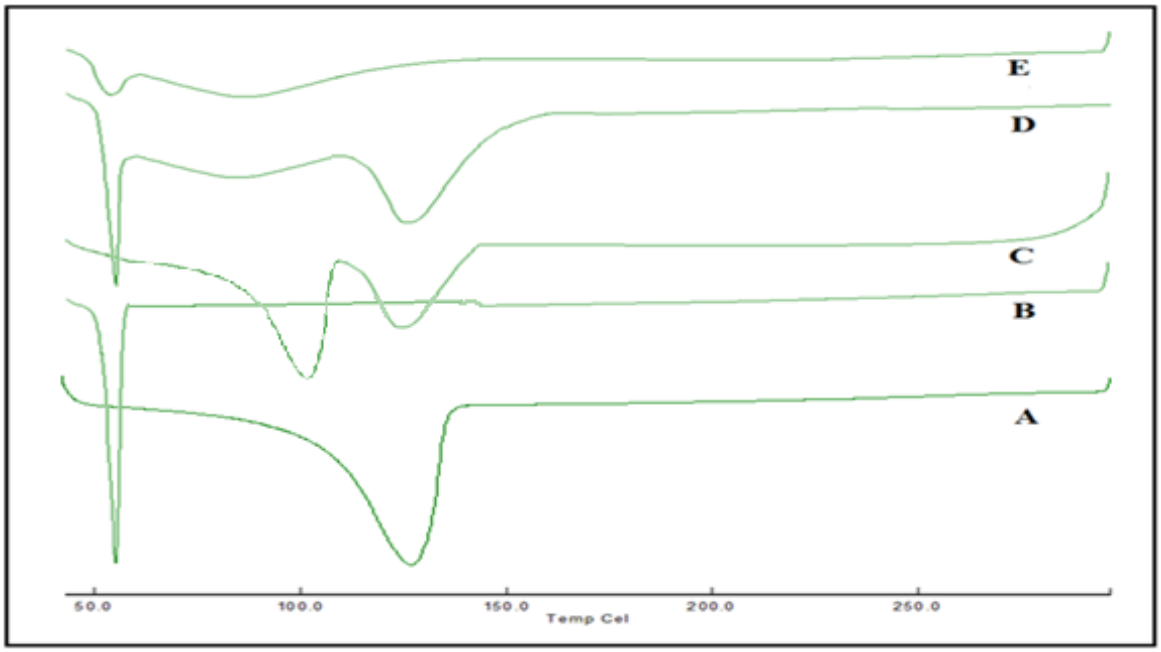

Figure 4. DSC thermogram of Qu-loaded nanoparticles **(A)** Quercetin, **(B)** Poloxamer-188, **(C)** Eudragit S100, **(D)** Physical mixture, **(E)** Quercetin nanoformulation.

3.2.4. X-ray diffraction (XRD)

The appearance of multiple distinct peaks at 12°, 16°, 25°, 28°, and 30° in the X-ray patterns of quercetin indicates its high degree of crystallinity. (Figure 5A), but poloxamer 188 has distinct peaks at 2°, 19°, and 24° (Figure 5B). Eudragit S100 has three XRD peaks, each corresponding to two distinct crystalline structures. The anhydrous crystalline structure peaks at 15°, whereas the hydrated crystalline structure peaks at 10° (or two peaks at 8 and 12°). Due to its amorphous form, Eudragit S100 also has a large peak about Eudragit S100 at 20°, matching crystallographic planes (Figure 5C) [50, 51]. When compared to the pure forms, diffraction angle 2= (9°, 18°, 20°, 24°, and 36°) demonstrated that absorbed into the nanoparticles as in an amorphous state. (Figure 5D) As a result, the XRD quercetin fingerprints results support the DSC findings that quercetin crystallinity was reduced in the Qu-loaded nanoparticles with lower enthalpy and melting temperatures, showing that it was encapsulated within the Eudragit S100 nanoformulation [50.51].

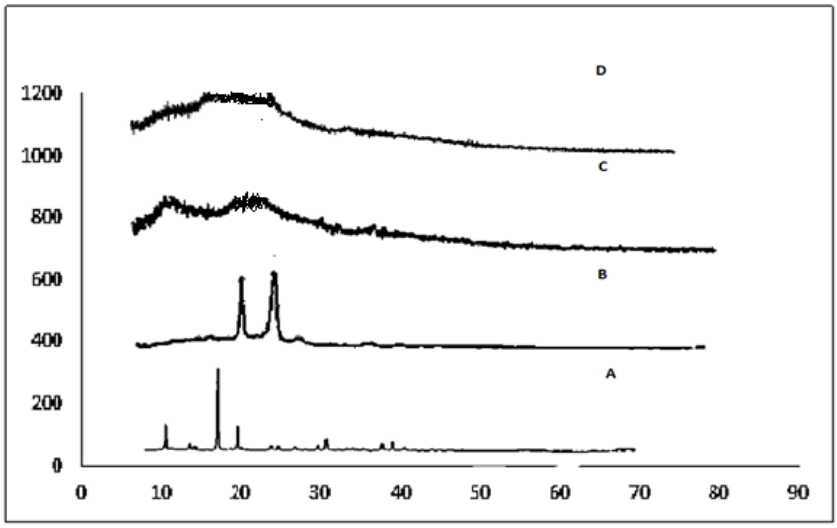

Figure 5: XRD Pattern of Qu-loaded nanoparticles **(A)** Quercetin, **(B)** Poloxamer 188, **(C)** Eudragit S100, **(D)** Quercetin nanoformulation.

3.2.5. Entrapment efficiency (EE) and loading content (LC).

Changes in Eudragit S 100 and poloxamer 188 concentrations affect encapsulation efficiency and loading content. We chose 2.4% Eudragit S 100 and 0.1% poloxamer 188 concentrations based on the influence of particle size and zeta potential. The quercetin in nanoformulation affects the EE and LC. Increasing the concentration of chitosan and poloxamer 407 was found to increase the EE and LC formulation to a specific concentration. The formulation of nanoparticles with Entrapment Efficiency (%) = 76.80 % and Loading Capacity (%) = 3.10 %.

3.2.6. *In vitro* release study.

In a vitro-release pattern, the formulation of quercetin (Figure 6) demonstrates superior drug release at 77.16 percent after 12 hours in a sustained manner. The optimum linearity connection in K-Peppas was discovered by fitting the data with n=2.350, and the cumulative drug release plot was determined to be linear (super case II transport). Non-Fickian release occurs when n is between 0.5 and 1.0, whereas Fickian diffusion occurs when n = 0.5. Case II transport is indicated when n = 1 for zero-order release; however, if n > 1, super case II transport is indicated. The release patterns in the test conditions indicate a short burst of quercetin followed by a steady release. On the hydrophilic Eudragit S100 lead, quercetin's hydrophobicity may have prevented excessive surface binding to small burst release, resulting in delayed release due to unique interactions between Qu-loaded nanoparticles [52].

The linearity for zero order y=7.9878x-4.4891 with R2= 0.979, for first-order y=-0.086x+2.1588 with R2=0.9284 for Higuchi y=35.679x-38.674 with R2=0.9435, for Hixson Crowell y=0.101x+2.677 with R2=0.612, and for In K-Peppas, model the best linearity relationship was found by y=1.108x+07564 with R2=0.9819.

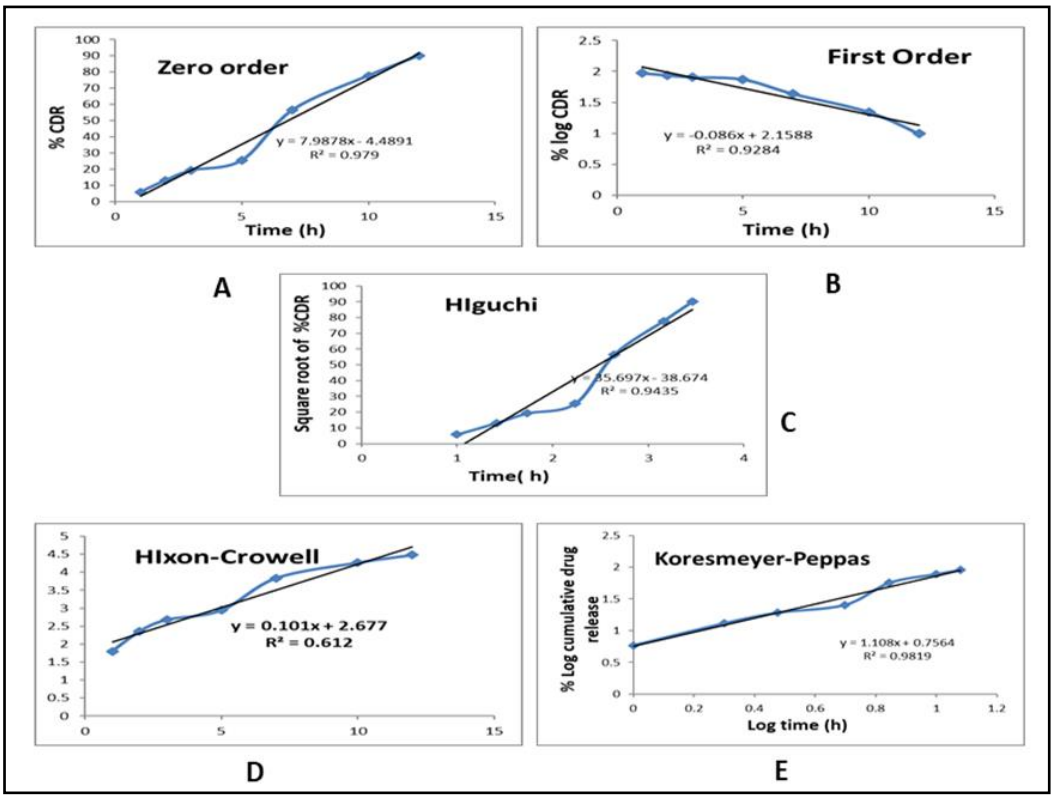

Figure 6. *In-vitro* drug release plots in different kinetic models **(A)** zero order **(B)** First order **(C)** Koresmeyer-Peppas **(D)** HIxob-Crowell **(E)** Higuchi.

The formulation of quercetin *in-vitro* release pattern has been proven to have better drug release 88.16 % after 12 hours in a sustained manner, as shown in the following table no 2.

Table 2. *In-vitro* drug releases in different kinetic models

Kinetic Models	Zero-order			First-order			Higuchi	Hixon-Crowell
Sr. No.	Time (h)	%CR	Log (time)	Log (%CR)	% DR Rem.	Log % DR	SQRT time	Cube Root of DR
1	1	5.85	0	0.7671	94.15	1.97382	1	1.80185
2	2	13.08	0.3013	1.1166	86.92	1.93912	1.4142	2.356148
3	3	19.21	0.4771	1.2835	80.79	1.90736	1.7320	2.678197
4	5	25.46	0.6989	1.4058	74.54	1.87239	2.2360	2.941843
5	7	56.56	0.8450	1.7525	43.44	1.63789	2.6457	3.838573
6	10	77.81	1	1.8910	22.19	1.34616	3.1622	4.269187
7	12	90.12	1.0791	1.9548	9.88	0.99476	3.4641	4.483396

3.2.7. Assessment of *in-vitro* antidiabetic activity.

The yeast cell glucose uptake method was used to assess the antidiabetic efficacy of Qu-loaded nanoparticles. The transfer of glucose throughout the yeast cell may be facilitated by the diffusion mechanism. When most of the glucose in the cell is utilized or transformed into other metabolites, the concentration in the cell drops. This situation encourages the cell to take in a lot of glucose. In the current situation, including Qu-loaded nanoparticles may allow high glucose transport within the cell down the concentration gradient.

The glucose uptake activity of samples (Control, Standard Metformin, and Qu-loaded nanoparticles) by yeast cells is shown in the table below. This approach determines how much glucose is left in the medium. Qu-loaded nanoparticles had a percentage glucose uptake of 30.13, while metformin had a percentage of [42, 53].

Table 3. Glucose uptake by yeast cells.

Sample code	Concentration mM	Glucose uptake by Yeast cells	
		Absorbance at 565 nm	% Glucose uptake by Yeast cells
Control	-	0.73	-
Standard(Metformin)	25	0.34	**53.42**
Sample(Qu-loaded nanoparticles)	25	0.51	**30.13**

The glucose uptake of yeast cells may be different from that of other eukaryotic or human body cells. Rather than the mediation of a phosphotransferase enzyme system or any other undiscovered activity, glucose transport across the yeast membrane may be facilitated diffusion. Several factors, including glucose levels inside the cells and subsequent glucose metabolism, influence glucose uptake by yeast cells. The internal glucose concentration will drop if most internal sugar is rapidly converted into other metabolites, favoring high glucose absorption into the cell. Increased glucose absorption in yeast cells was found after treatment with quercetin-loaded nanoparticles.

4. Conclusions

Herbal formulations are considered more effective than allopathic drugs because they have fewer side effects, are less expensive, are safer, and are more readily available. Inhibition of carbohydrate hydrolyzing enzymes (-amylase and -glucosidase) is one of the therapeutic strategies for decreasing postprandial hyperglycemia. According to the results, quercetin was

successfully synthesized into stabilized Qu-loaded nanoparticles, demonstrating greater benefits than the regular metformin drug. FT-IR, DSC, and XRD analysis showed no chemical interaction between quercetin and the Eudragit S100 polymer.

The current study shows the nanoformulation antidiabetic effectiveness and indicates possible pathways for controlling blood glucose levels by inhibiting -amylase and -glucosidase and increasing glucose uptake activity. As a result, this study suggested that the developed stable formulation might be used as an antidiabetic regimen. As a result, more *in vitro* and *in vivo* research is needed to determine its multiple real targets and prove its antidiabetic effectiveness. Furthermore, a prescreening investigation for identifying and characterizing Qu-loaded nanoparticles is advised.

Funding

This review received no external funding.

Acknowledgments

The author(s) express their deep sense of gratitude towards Ashokrao Mane College of Pharmacy, Peth Vadgaon, Kolhapur, Maharashtra, (India) for the provision of obligatory facilities to carry out present research work. Dr. Riyaz Ali M. Osmani, Department of Biosciences and Bioengineering (BSBE), Indian Institute of Technology Bombay (IITB), Mumbai, is gratefully acknowledged for his outstanding contributions and constructive ideas.

Conflicts of Interest

The authors report no conflicts of interest. The authors alone are responsible for the content and writing of this article.

References

1. Dey, L.; Attele, A.S.; Yuan, C.-S. Alternative therapies for type 2 diabetes. *Alternative medicine review* **2002**, *7*, 45-58, https://pubmed.ncbi.nlm.nih.gov/11896745/.
2. Wild, S.; Roglic, G.; Green, A.; Sicree, R.; King, H. Global prevalence of diabetes: estimates for the year 2000 and projections for 2030. *Diabetes care* **2004**, *27*, 1047-1053, https://doi.org/10.2337/diacare.27.5.1047.
3. Gurudeeban, S.; Satyavani, K.; Ramanathan, T. Alpha-glucosidase inhibitory effect and enzyme kinetics of coastal medicinal plants. ||| *Bangladesh Journal of Pharmacology* **2012**, *7*, 186-191, 186-191, https://doi.org/10.3329/bjp.v7i3.11499.
4. Marton, L.T.; Pescinini-e-Salzedas, L.M.; Camargo, M.E.C.; Barbalho, S.M.; Haber, J.F.d.S.; Sinatora, R.V.; Detregiachi, C.R.P.; Girio, R.J.; Buchaim, D.V.; Cincotto dos Santos Bueno, P.J.F.i.e. The effects of curcumin on diabetes mellitus: a systematic review. **2021**, *12*, 669448, https://doi.org/10.3389%2Ffendo.2021.669448.
5. Thengyai, S.; Thiantongin, P.; Sontimuang, C.; Ovatlarnporn, C.; Puttarak, P. α-Glucosidase and α-amylase inhibitory activities of medicinal plants in Thai antidiabetic recipes and bioactive compounds from Vitex glabrata R. Br. stem bark. *Journal of herbal medicine* **2020**, *19*, 100302, https://doi.org/10.1016/j.hermed.2019.100302.
6. Mayur, B.; Sancheti, S.; Shruti, S.; Sung-Yum, S. Antioxidant and-glucosidase inhibitory properties of Carpesium abrotanoides L. *Journal of Medicinal Plants Research* **2010**, *4*, 1547-1553, https://academicjournals.org/article/article1380703440_Mayur%20et%20al%20PDF.pdf.
7. Ojo, M.C.; Osunsanmi, F.O.; Zaharare, G.E.; Mosa, R.A.; Cele, N.D.; Oboh, M.O.; Opoku, A.R. *In-vitro* Antidiabetic and Antioxidant Efficacy of Methanolic Extract of Encephalartos ferox leaves. *Pharmacognosy Journal* **2019**, *11*, http://dx.doi.org/10.5530/pj.2019.11.71.
8. Mohammadi, E.; Behnam, B.; Mohammadinejad, R.; Guest, P.C.; Simental-Mendía, L.E.; Sahebkar, A.J.S.o.B.; Turmeric, N.T.i.A.R.i.I.F.o.; Curcumin. Antidiabetic properties of curcumin: insights on new mechanisms. **2021**, 151-164, https://doi.org/10.1007/978-3-030-56153-6_9.

9. Rebello, C.J.; Beyl, R.A.; Lertora, J.J.; Greenway, F.L.; Ravussin, E.; Ribnicky, D.M.; Poulev, A.; Kennedy, B.J.; Castro, H.F.; Campagna, S.R.J.D., Obesity; et al. Safety and pharmacokinetics of naringenin: A randomized, controlled, single-ascending-dose clinical trial. **2020**, *22*, 91-98, https://doi.org/10.1111/dom.13868.
10. Imran, M.; Saeed, F.; Hussain, G.; Imran, A.; Mehmood, Z.; Gondal, T.A.; El-Ghorab, A.; Ahmad, I.; Pezzani, R.; Arshad, M.U.J.F.S.; et al. Myricetin: A comprehensive review on its biological potentials. **2021**, *9*, 5854-5868, https://doi.org/10.1002/fsn3.2513.
11. Qin, J.; Chen, J.; Peng, F.; Sun, C.; Lei, Y.; Chen, G.; Li, G.; Yin, Y.; Lin, Z.; Wu, L.J.J.o.E. Pharmacological activities and pharmacokinetics of liquiritin: a review. **2022**, *293*, 115257, https://doi.org/10.1016/j.jep.2022.115257.
12. Srivastava, A.K.; Maurya, R. Antihyperglycemic activity of compounds isolated from Indian medicinal plants. **2010**, *48*, 294-298, https://pubmed.ncbi.nlm.nih.gov/21046984/.
13. Chattopadhyay, R. A comparative evaluation of some blood sugar lowering agents of plant origin. *Journal of ethnopharmacology* **1999**, *67*, 367-372, https://doi.org/10.1016/S0378-8741(99)00095-1.
14. Faisal Lutfi, M.; Abdel-Moneim, A.-M.H.; Alsharidah, A.S.; Mobark, M.A.; Abdellatif, A.A.; Saleem, I.Y.; Al Rugaie, O.; Mohany, K.M.; Alsharidah, M.J.M. Thymoquinone lowers blood glucose and reduces oxidative stress in a rat model of diabetes. **2021**, *26*, 2348, https://doi.org/10.3390/molecules26082348.
15. Pennathur, S.; Heinecke, J.W. Mechanisms of oxidative stress in diabetes: implications for the pathogenesis of vascular disease and antioxidant therapy. *Front Biosci* **2004**, *9*, 565-574, https://doi.org/10.2741/1257.
16. Thilagam, E.; Parimaladevi, B.; Kumarappan, C.; Mandal, S.C. α-Glucosidase and α-amylase inhibitory activity of Senna surattensis. *Journal of acupuncture and meridian studies* **2013**, *6*, 24-30, https://doi.org/10.1016/j.jams.2012.10.005.
17. Kambale, E.K.; Quetin-Leclercq, J.; Memvanga, P.B.; Beloqui, A.J.P. An Overview of Herbal-Based Antidiabetic Drug Delivery Systems: Focus on Lipid-and Inorganic-Based Nanoformulations. **2022**, *14*, 2135, https://doi.org/10.3390/pharmaceutics14102135.
18. Luo, W.; Zhao, M.; Yang, B.; Ren, J.; Shen, G.; Rao, G. Antioxidant and antiproliferative capacities of phenolics purified from Phyllanthus emblica L. fruit. *Food Chemistry* **2011**, *126*, 277-282, https://doi.org/10.1016/j.foodchem.2010.11.018.
19. Erlund, I. Review of the flavonoids quercetin, hesperetin, and naringenin. Dietary sources, bioactivities, bioavailability, and epidemiology. *Nutrition research* **2004**, *24*, 851-874, https://doi.org/10.1016/j.nutres.2004.07.005.
20. Baltina, L.; Sapozhnikova, T.; Gabdrakhmanova, S.; Makara, N.; Khisamutdinova, R.Y.; Baltina, J., LA; Petrova, S.; Saifullina, D.; Kondratenko, R.J.P.C.J. Hypoglycemic activity of Glycyrrhizic acid and some of its derivatives in the alloxan diabetes model in rats. **2021**, *55*, 340-344, https://doi.org/10.1007/s11094-021-02424-x.
21. Yao, L.H.; Jiang, Y.-M.; Shi, J.; Tomas-Barberan, F.; Datta, N.; Singanusong, R.; Chen, S. Flavonoids in food and their health benefits. *Plant foods for human nutrition* **2004**, *59*, 113-122, https://doi.org/10.1007/s11130-004-0049-7.
22. Rauf, A.; Imran, M.; Khan, I.A.; ur-Rehman, M.; Gilani, S.A.; Mehmood, Z.; Mubarak, M.S. Anticancer potential of quercetin: A comprehensive review. *Phytotherapy Research* **2018**, *32*, 2109-2130, https://doi.org/10.1002/ptr.6155.
23. Liao, H.; Tang, M.; Luo, L.; Li, C.; Chiclana, F.; Zeng, X.-J. A bibliometric analysis and visualization of medical big data research. *Sustainability* **2018**, *10*, 166, https://doi.org/10.3390/su10010166.
24. Xu, L.; Wang, X.; Liu, Y.; Yang, G.; Falconer, R.J.; Zhao, C.-X.J.A.N.R. Lipid nanoparticles for drug delivery. **2022**, *2*, 2100109, https://doi.org/10.1002/anbr.202100109.
25. Kyriakoudi, A.; Spanidi, E.; Mourtzinos, I.; Gardikis, K.J.P. Innovative delivery systems loaded with plant bioactive ingredients: Formulation approaches and applications. **2021**, *10*, 1238, https://doi.org/10.3390/plants10061238.
26. Xu, Y.; Michalowski, C.B.; Beloqui, A.J.C.O.i.C.; Science, I. Advances in lipid carriers for drug delivery to the gastrointestinal tract. **2021**, *52*, 101414, https://doi.org/10.1016/j.cocis.2020.101414.
27. Patil, P.; Killedar, S. Chitosan and glyceryl monooleate nanostructures containing gallic acid isolated from amla fruit: targeted delivery system. *Heliyon* **2021**, *7*, e06526, https://doi.org/10.1016/j.heliyon.2021.e06526.
28. Gulbake, A.; Jain, S.K. Chitosan: a potential polymer for colon-specific drug delivery system. *Expert opinion on drug delivery* **2012**, *9*, 713-729, https://doi.org/10.1517/17425247.2012.682148.
29. Patil, P.; Killedar, S. Formulation and characterization of gallic acid and quercetin chitosan nanoparticles for sustained release in treating colorectal cancer. *Journal of Drug Delivery Science and Technology* **2021**, *63*, 102523, https://doi.org/10.1016/j.jddst.2021.102523.
30. Li, L.; Gao, H.; Lou, K.; Luo, H.; Hao, S.; Yuan, J.; Liu, Z.; Dong, R.J.C.; Science, T. Safety, tolerability, and pharmacokinetics of oral baicalein tablets in healthy Chinese subjects: A single-center, randomized, double-blind, placebo-controlled multiple-ascending-dose study. **2021**, *14*, 2017-2024, https://doi.org/10.1111/cts.13063.

31. Abedimanesh, N.; Asghari, S.; Mohammadnejad, K.; Daneshvar, Z.; Rahmani, S.; Shokoohi, S.; Farzaneh, A.H.; Hosseini, S.H.; Jafari Anarkooli, I.; Noubarani, M.J.N.; et al. The antidiabetic effects of betanin in streptozotocin-induced diabetic rats through modulating AMPK/SIRT1/NF-κB signaling pathway. **2021**, *18*, 1-13, https://doi.org/10.1186/s12986-021-00621-9.
32. Winarti, L.; Sari, L.O.R.K.; SAMSURI, E.U.U.; Ayu, D. Formulation and Antioxidant Property of Bitter Melon Seed Oil Loaded into SNEDDS as a Nutraceutical. **2021**, https://jurnal.ugm.ac.id/v3/IJP/article/view/1334.
33. Patil, P.; Killedar, S. Green Approach Towards Synthesis and Characterization of GMO/Chitosan Nanoparticles for *In vitro* Release of Quercetin: Isolated from Peels of Pomegranate Fruit. *Journal of Pharmaceutical Innovation* **2021**, 1-14, https://doi.org/10.1007/s12247-021-09558-1.
34. Wu, T.-H.; Yen, F.-L.; Lin, L.-T.; Tsai, T.-R.; Lin, C.-C.; Cham, T.-M. Preparation, physicochemical characterization, and antioxidant effects of quercetin nanoparticles. *International journal of pharmaceutics* **2008**, *346*, 160-168, https://doi.org/10.1016/j.ijpharm.2007.06.036.
35. Dudhani, A.R.; Kosaraju, S.L. Bioadhesive chitosan nanoparticles: Preparation and characterization. *Carbohydrate polymers* **2010**, *81*, 243-251, https://doi.org/10.1016/j.carbpol.2010.02.026.
36. Yu, S.-H.; Mi, F.-L.; Pang, J.-C.; Jiang, S.-C.; Kuo, T.-H.; Wu, S.-J.; Shyu, S.-S. Preparation and characterization of radical and pH-responsive chitosan–gallic acid conjugate drug carriers. *Carbohydrate polymers* **2011**, *84*, 794-802, https://doi.org/10.1016/j.carbpol.2010.04.035.
37. Vozza, G.; Danish, M.; Byrne, H.J.; Frías, J.M.; Ryan, S.M. Application of Box-Behnken experimental design for the formulation and optimisation of selenomethionine-loaded chitosan nanoparticles coated with zein for oral Delivery. *International journal of pharmaceutics* **2018**, *551*, 257-269, https://doi.org/10.1016/j.ijpharm.2018.08.050.
38. Pandit, A.A.; Dash, A.K. Surface-modified solid lipid nanoparticulate formulation for ifosfamide: development and characterization. *Nanomedicine* **2011**, *6*, 1397-1412, https://doi.org/10.2217/nnm.11.57.
39. Kumari, A.; Yadav, S.K.; Yadav, S.C. Biodegradable polymeric nanoparticles based drug delivery systems. *Colloids and Surfaces B: Biointerfaces* **2010**, *75*, 1-18, https://doi.org/10.1016/j.colsurfb.2009.09.001.
40. Patra, A.; Satpathy, S.; Shenoy, A.K.; Bush, J.A.; Kazi, M.; Hussain, M.D. Formulation and evaluation of mixed polymeric micelles of quercetin for treatment of breast, ovarian, and multidrug resistant cancers. *International journal of nanomedicine* **2018**, *13*, 2869, https://doi.org/10.2147/ijn.s153094.
41. Park, S.N.; Jo, N.R.; Jeon, S.H. Chitosan-coated liposomes for enhanced skin permeation of resveratrol. *Journal of industrial and engineering chemistry* **2014**, *20*, 1481-1485, https://doi.org/10.1016/j.jiec.2013.07.035.
42. Vijayakumar, A.; Baskaran, R.; Jang, Y.S.; Oh, S.H.; Yoo, B.K. Quercetin-loaded solid lipid nanoparticle dispersion with improved physicochemical properties and cellular uptake. *Aaps Pharmscitech* **2017**, *18*, 875-883, https://doi.org/10.1208/s12249-016-0573-4.
43. Ramadon, D.; Anwar, E.; Harahap, Y. *In vitro* penetration and bioavailability of novel transdermal quercetin-loaded ethosomal gel. *Indian journal of pharmaceutical sciences* **2018**, *79*, 948-956, http://dx.doi.org/10.4172/pharmaceutical-sciences.1000312.
44. Santhiya, N.; Priyanga, S.; Hemmalakshmi, S.; Devaki, K. Phytochemical analysis, Anti inflammatory activity, *In vitro* antidiabetic activity and GC-MS profile of Erythrina variegata L. bark. *J Appl Pharm Sci* **2016**, *6*, 147-155, http://dx.doi.org/10.7324/JAPS.2016.60722.
45. Jawarkar, S.V.; Jat, R.K. INVITRO-ANTIDIABETIC, ACTIVITY OF ETHANOL EXTRACT OF GLOCHIDION ELLIPTICUM. **2016**, https://wjpr.s3.ap-south-1.amazonaws.com/article_issue/1467278656.pdf.
46. Anitha, T.; Pakutharivu, T.; Nirubama, K.; Akshaya, V. Phytochemical evaluation and *In vitro* antidiabetic efficiency of isopropanolic leaf extract of pimenta racemosa. *Kongunadu Research Journal* **2020**, *7*, 50-55, https://doi.org/10.26524/krj.2020.21.
47. Kamaly, N.; Yameen, B.; Wu, J.; Farokhzad, O.C. Degradable controlled-release polymers and polymeric nanoparticles: mechanisms of controlling drug release. *Chemical Reviews* **2016**, *116*, 2602-2663, https://doi.org/10.1021/acs.chemrev.5b00346.
48. Kumari, A.; Yadav, S.K.; Pakade, Y.B.; Singh, B.; Yadav, S.C. Development of biodegradable nanoparticles for Delivery of quercetin. *Colloids and Surfaces B: Biointerfaces* **2010**, *80*, 184-192, https://doi.org/10.1016/j.colsurfb.2010.06.002.
49. Han, Q.; Wang, X.; Cai, S.; Liu, X.; Zhang, Y.; Yang, L.; Wang, C.; Yang, R. Quercetin nanoparticles with enhanced bioavailability as multifunctional agents toward amyloid induced neurotoxicity. *Journal of Materials Chemistry B* **2018**, *6*, 1387-1393, https://doi.org/10.1039/C7TB03053C.
50. Khor, C.M.; Ng, W.K.; Chan, K.P.; Dong, Y. Preparation and characterization of quercetin/dietary fiber nanoformulations. *Carbohydrate polymers* **2017**, *161*, 109-117, https://doi.org/10.1016/j.carbpol.2016.12.059.
51. Hosseini, S.F.; Zandi, M.; Rezaei, M.; Farahmandghavi, F. Two-step method for encapsulation of oregano essential oil in chitosan nanoparticles: preparation, characterization and *In vitro* release study. *Carbohydrate polymers* **2013**, *95*, 50-56, https://doi.org/10.1016/j.carbpol.2013.02.031.

52. Sahle, F.F.; Balzus, B.; Gerecke, C.; Kleuser, B.; Bodmeier, R. Formulation and *In vitro* evaluation of polymeric enteric nanoparticles as dermal carriers with pH-dependent targeting potential. *European Journal of Pharmaceutical Sciences* **2016**, *92*, 98-109, https://doi.org/10.1016/j.ejps.2016.07.004.